c = elementary gravity wave celerity;
F = Froude number;
g = gravitational force per unit mass;
H = total head;
k = constant defining width of channel cross section;
k_b = constant defining width of breach section;
M = momentum content per unit mass density of volume element in numerical scheme;
m = exponent defining shape of channel and breach cross sections;
n = Manning roughness coefficient;
P = hydrostatic force on cross section per unit weight of fluid;
p = ratio of undisturbed depth in reservoir to depth at section 2 in the breach;
Q = volumetric flowrate;
Q_{max} = volumetric flowrate corresponding to the Ritter solution for total failure;
R_x = term accounting for nonprismatic channel in Vasiliev method;
r = ratio of depth at section 3 in breach to depth at section 2 in breach;
r_{min} = minimum value of r for submerged flow;
S_0 = bottom slope;
S_f = hydraulic resistance slope;
s = ratio of depth at section 4 in breach to depth at section 3 in breach;
s_{max} = maximum value of s for submerged flow;
t = time;
V = fluid velocity;
$\forall$ = volume of fluid element in numerical scheme;
w = speed of motion of a face of volume element in numerical scheme;
x = distance along channel;
y = fluid depth above channel invert;
β = ratio of breach width to channel width;
γ = weight of fluid per unit volume;
δt = time interval;
δx = space increment;
η = variable of integration;
ρ = fluid density;
χ = stability parameter in Vasiliev method; and
ω = Escoffier stage variable.

Subscripts

i = time interval index;
k = space increment index; and
N = maximum value of space increment index.

Turbulent Boundary Layer in Wave-Current Motion

By Jørgen Fredsøe[1]

Abstract: The mean current velocity profile in the combined wave-current motion is calculated by use of the depth-integrated momentum equation. The velocity distribution is assumed to be logarithmic inside as well as outside the wave boundary layer, but with different slopes. Hereby, it is possible to describe the flow in the whole range from the pure wave motion (without any mean current) to the pure current motion (without any waves). The theory covers an arbitrary angle between wave propagation direction and mean current direction.

Introduction

The flow conditions near the bed in combined wave-current motion is of interest inside several fields of hydraulic engineering. For instance, the near-bed flow is fundamental for evaluating the sediment transport rate in combined wave-current motion, where the sediment normally is picked up by the waves and transported by the mean current. In recent years attention has been paid to the near-bed flow for evaluation of forces on near-bed structures like off-shore pipelines. Finally, knowledge of the flow in the turbulent boundary layer is of interest for the evaluation of energy dissipation in waves.

Review of Theoretical Developments

The work done until now on wave boundary layers can be mainly divided into two parts: (1) The work done on the pure oscillation flow; and (2) extension of theories in item 1 to cover the combined wave-current motion.

Oscillating Boundary Layer.—One of the first attempts to describe the pure oscillating turbulent boundary layer by a mathematical model was done by Kajiura (10). He adopted the eddy-viscosity concept in a three-layer model: In the small inner layer the eddy viscosity, ϵ, was taken as a constant. In an overlap layer, ϵ was assumed to vary linearly with the distance from the bed and, finally, ϵ was kept constant from a certain distance away from the bed (the outer layer). By use of the equation of motion, Kajiura obtained a rather laborious analytical-numerical solution. Recently, Brevik (4) has simplified the analysis by Kajiura by avoiding the inner layer, where ϵ was kept constant. Hereby, it was possible to reduce the calculations of Kajiura. The amount of work inherent in the analytical calculations is, however, still considerable.

Kajiura and Brevik tested their analytical results against the experimental work done by Jonsson (7) [see also Jonsson and Carlsen (8)] and

[1]Assoc. Prof., Inst. Hydrodynamics and Hydr. Engrg., Lyngby, Denmark (ISVA).

Note.—Discussion open until January 1, 1985. To extend the closing date one month, a written request must be filed with the ASCE Manager of Technical and Professional Publications. The manuscript for this paper was submitted for review and possible publication on August 19, 1982. This paper is part of the *Journal of Hydraulic Engineering*, Vol. 110, No. 8, August, 1984. ©ASCE, ISSN 0733-9429/84/0008-1103/$01.00. Paper No. 19055.

obtained reasonable agreement. However, three shortcomings in Kajiura's and Brevik's theory must be mentioned: (1) They did not take into account that the eddy viscosity is a function of *time*, as well as of the distance from the wall; (2) the thickness of the wave boundary layer was also taken as a time-independent quantity; and, finally, (3) the variation in bed shear stress was assumed to be sinusoidal.

Some of these shortcomings were removed in a later model by Jonsson and Carlsen (8) who considered the problem from a different point of view:

By using the momentum equation (integrated over depth) and the assumption that the velocity distribution in the boundary layer is logarithmic, a reasonable estimate for the friction factor was obtained in the case of a rough wall. However, because the momentum equation was integrated over a wave period it was not possible to describe the detailed variation in bed shear stress and the phase between maximum bed shear stress and maximum outer velocity. Further, the variation in boundary layer thickness with time was partly neglected so that a constant from the integration had to be determined from experiments.

Finally, the work by Bakker (1) must be mentioned. Bakker introduced a mixing length hypothesis like that of Prandtl and assumed that the mixing length was proportional with the distance from the bed. Combined with the equation of motion, the mixing-length theory involves the solution of a second order nonlinear partial differential equation of the type

$$\frac{\partial p}{\partial t} = \kappa y \frac{\partial^2 (p|p|)}{\partial y^2} \quad \ldots\ldots (1)$$

in which p = the friction velocity (equal to the square root of shear); y = the distance from the bed; t = the time; and $\kappa = 0.4$ (von Kármán's constant). The numerical work is rather complicated and the physical assumptions introduced by Bakker cannot be shown to be superior to other assumptions because the mixing length assumption may be questionable in unsteady flow.

Combined Wave-Current Motion.—Most of the work done on the combined wave-current motion follows the same line as that for the pure wave motion. Lundgren (13) utilized the measurements of the eddy viscosity in the pure wave boundary layer from Ref. 7 to establish a theory for the combined motion by use of the eddy-viscosity concept. Here, the eddy viscosity was taken as the mean eddy viscosity during one wave period. The shortcoming of Lundgren's model is that it is a time averaged model which does not describe the variations with time of the boundary layer. A simplified model of Lundgren's theory was later developed by Fredsøe (5).

Grant and Madsen (6) developed a more detailed model of the flow than that by Lundgren: By also adopting the eddy viscosity concept they described the combined motion in the boundary layer from the equation of motion. The calculations of Madsen and Grant are rather laborious and the model has the same three shortcomings as that of Kajiura and Brevik concerning the pure oscillating wave boundary layer: The eddy viscosity is not taken to be a function of time, the boundary layer thickness is taken as a constant, and all variations with time are assumed to be sinusoidal.

The model by Grant and Madsen, however, pointed out one important feature: The influence of the wave on the steady current above the wave boundary layer is an apparent increase in the roughness experienced by the current. This could, in fact, also be concluded from Ref. 13.

Some of the shortcomings in the work by Grant and Madsen are avoided in the paper by Bakker and Doorn (2). Their paper is an extension of the work by Bakker (1), still applying the mixing length hypothesis, so they end up with an equation like Eq. 1. In order to solve Eq. 1, boundary conditions are needed. These, however, are not known in advance, so an iterative procedure must be applied, which makes the solution of the problem tedious. The improvement introduced through the work by Bakker and Doorn is the inclusion of the time variation in the eddy viscosity by not applying this concept directly in the calculations. However, as in the case of a pure oscillating boundary layer, the assumption of a mixing length hypothesis in a strongly unsteady flow may be questionable.

The work by Bakker and Doorn is restricted to the two-dimensional case (in which the direction of wave propagation and mean current is parallel), while Grant and Madsen's model covers the three-dimensional situation.

Scope of Present Work

The main problem arising in the combined motion of waves and a current is that a thin turbulent wave boundary layer develops at the sea bed due to the oscillatory wave movement. On the other hand, the flow formed by the more steady current is turbulent over the entire water depth and does not have the same boundary layer character as that originating from the waves. Thus we have two different types of turbulence, one originating from the wave motion and another, originating from the mean current. The interaction of the two kinds of turbulence is highly nonlinear.

For reasons of simplicity, the present theory is developed in two steps: First we consider the pure oscillating wave boundary layer and, secondly, the combined wave-current motion is considered.

The theoretical development follows the line of Jonsson and Carlsen by applying the equation of momentum in the boundary layer and assuming the velocity profile to be logarithmic. In case of no mean current motion, the main idea is to study the development of the boundary layer when the water from total rest is exposed to a periodic motion outside the boundary layer. Hereby, the effect of eddies formed by the previous movement is disregarded.

This is a physically reasonable assumption if the time scale for the change in outer velocity (equal to the wave-period) is much larger than the time scale for the decay of eddies formed in the wave boundary layer. This will normally be the case in nature because the wave boundary layer is very thin, so the side of the eddies is rather small. It must be pointed out, however, that the theory breaks down at a very fast

frequency, in which case the memory effects in the turbulence formed in the wave boundary layer are of importance.

Development of Wave Boundary Layer Without Any Mean Current

Outside the wave boundary layer, the velocity is assumed to be a periodic motion with the velocity

$$v_0 = v_{1m} \sin(\omega t) \quad \ldots\ldots (2)$$

in which v_{1m} = maximum velocity occurring outside the boundary layer from the wave motion (calculated from potential theory); and ω = angular frequency (= $2\pi/T$, T = wave period).

Rough Wall.—In the case of a rough wall, the velocity profile in the boundary layer is assumed to be given by

$$\frac{U}{U_f} = \frac{1}{\kappa} \ln \frac{y}{\frac{k}{30}} \quad \ldots\ldots (3)$$

in which k = the bed roughness; κ = the von Kármán constant (= 0.40); U_f = friction velocity; and y = the distance from the bed. In this case, the momentum equations reads

$$-\frac{\tau_0}{\rho} = -U_f^2 = -\int_{k/30}^{\delta+k/30} \frac{\partial}{\partial t}(U_0 - U)dy \quad \ldots\ldots (4)$$

in which τ_0 = bed shear stress; ρ = fluid density; δ = wave boundary layer thickness; and t = time.

It is convenient to introduce the upper limit in the integral to $\delta + k/30$ rather than δ (as is normally done), because $\delta = 0$ for $t = 0$.

The boundary condition at the top of the boundary layer is $y = \delta + k/30$: $U = U_0$ or, by the use of Eq. 3

$$\delta = \frac{k}{30}(e^z - 1) \quad \ldots\ldots (5)$$

$$\text{in which} \quad z = \frac{U_0}{U_f}\kappa \quad \ldots\ldots (6)$$

Now, the integral on the right-hand side of Eq. 4 can be carried out to

$$-U_f^2 = -\delta \frac{dU_0}{dt} + \frac{1}{\kappa}\frac{dU_f}{dt}\frac{k}{30}[e^z(z-1)+1] \quad \ldots\ldots (7)$$

by using Eqs. 3, 5, and 6. This relation can be converted into a differential equation in z, utilizing

$$\frac{dz}{dt} = \frac{z}{U_0}\frac{dU_0}{dt} - \frac{z}{U_f}\frac{dU_f}{dt} \quad \ldots\ldots (8)$$

which is obtained from Eq. 6.

Hereby, Eq. 7 can be written as (eliminating dU_f/dt)

$$\frac{dz}{d(\omega t)} = \beta \frac{\sin(\omega t)}{e^z(z-1)+1} - \frac{z(e^z - z - 1)}{e^z(z-1)+1}\frac{1}{U_0}\frac{dU_0}{d(\omega t)} \quad \ldots\ldots (9)$$

$$\text{in which} \quad \beta = \frac{30\kappa^2}{k}\frac{U_{1m}}{\omega} = 30\kappa^2\frac{a}{k} \quad \ldots\ldots (10)$$

in which a = the free stream particle amplitude. Normally, β is a very large quantity. Eq. 9 must be solved numerically. Because of the boundary condition $\delta = 0$ for $t = 0$, the boundary condition to z is $z = 0$ for $t = 0$ as seen from Eq. 5. Thus, at small values of t, Eq. 9 can be written as $dz/d(\omega t) = 2\beta(\omega t/z^2) - z/\omega t$ which has the solution

$$z = \sqrt[3]{\frac{6}{5}\beta}\,(\omega t)^{2/3} = t^* \quad \ldots\ldots (11)$$

In the numerical solution of Eq. 9, the time, t, has been replaced by t^*, defined in Eq. 11, in order to account for the singularity at $t = 0$.

In Fig. 1(*a*), the solution of Eq. 9 is shown for two different values of β (or a/k, cf. Eq. 10). From the knowledge of z it is easy to calculate the ratio U_f/U_{1m} (from Eqs. 2 and 6) as depicted in Fig. 1(*b*). The maximum value of this value defines the friction factor f_w by the relation

$$\sqrt{\frac{f_w}{2}} = \frac{U_{f,\max}}{U_{1m}} \quad \ldots\ldots (12)$$

in which f_w = a function of a/k as plotted in Fig. 2. The theoretical prediction fits well with experiments (11) for values of a/k larger than about 30. This is nearly the same value, below which it becomes questionable whether the velocity profile in the boundary layer is logarithmic (Ref. 8, pp. 57–58).

Like U_f, the boundary layer thickness varies with time as sketched in Fig. 1(*c*). Jonsson (9) defines the boundary layer thickenss δ_w equal to that occurring at $\omega t = \pi/2$. The variation in δ_w/a with a/k is given in Table 1. The present theoretical value of δ_1 is very near equal to twice the value suggested by Jonsson and Carlsen (see Fig. 12). This is probably due to their definition of δ_w, which they define as the minimum distance between the wall and the level where the velocity becomes equal to U_{1m}. As pointed out by Jonsson (9), $2\delta_w$ should in fact be a more consistent measure.

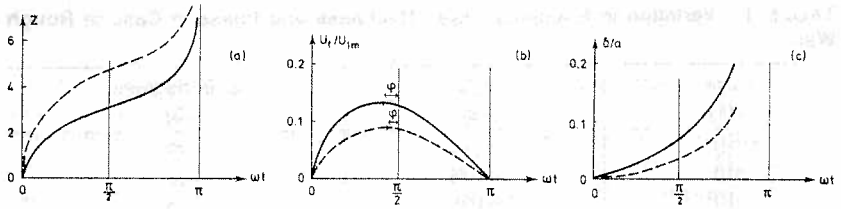

FIG. 1.—(*a*) Variation in z; (*b*) Variation in U_f/U_{1m}; (*c*) Variation in δ/a: With Time, ——: a/k = 10; ----: a/k = 100

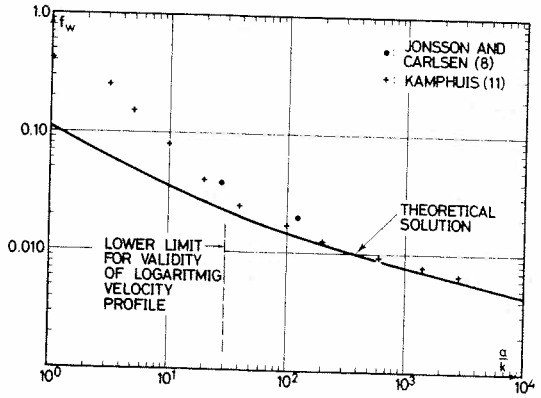

FIG. 2.—Variation in Friction Factor f_w with a/k in Case of Rough Bed

In Table 1, the phase, ϕ, between maximum bed shear stress and maximum velocity is also given.

Smooth Wall.—If the bed is hydraulically smooth, the velocity profile in a steady current is given by

$$\frac{U}{U_f} = 5.7 + \frac{1}{\kappa}\ln\left(\frac{U_f y}{\nu}\right) = \frac{1}{\kappa}\ln\left(\frac{9.8 U_f y}{\nu}\right) \quad \ldots\ldots (13)$$

in which ν = the kinematic viscosity. This expression is valid outside the viscous sublayer, where the profile is linear. The thickness of the viscous sublayer, δ_s, is given by $\delta_s = 11.7(\nu/U_f)$ in which the velocity profile is given by

$$\frac{U}{U_f} = \frac{U_f}{\nu} y \quad \ldots\ldots (14)$$

The simplest way to avoid the problem with two different velocity profiles in two different regions is to replace Eq. 13 by

$$\frac{U}{U_f} = \frac{1}{\kappa}\ln\left(\frac{9.8 U_f y}{\nu} + 1\right) \quad \ldots\ldots (15)$$

This profile is in the following assumed to be valid in the total region $0 \leqq y \leqq \delta$. As seen from Fig. 3, Eq. 15 is nearly identical with the correct

TABLE 1.—Variation in Boundary Layer Thickness and Phase in Case of Rough Wall

a/k (1)	δ_1/a (2)	ϕ, in degrees (3)
10^0	0.182	27
10^1	0.074	21
10^2	0.039	15
10^3	0.025	11
10^4	0.017	9

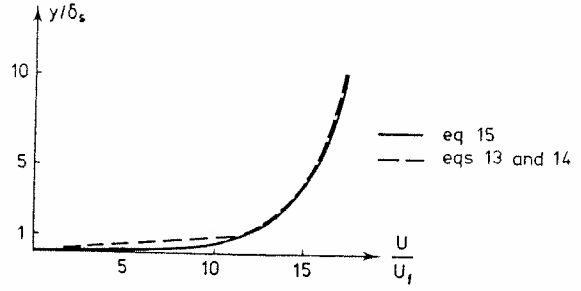

FIG. 3.—Correct Velocity Profile (Broken Line) in Flow Over Smooth Bed Compared with Approximated (Full Line)

profile except for a small deviation in the viscous sublayer. Eq. 15 is inserted in the momentum equation, which in the present case is

$$-U_f^2 = -\int_0^{\delta} \frac{\partial}{\partial t}(U_0 - U)dy \quad \ldots\ldots (16)$$

Hereby, the following differential equation in z, defined in Eq. 6, is obtained

$$\frac{dz}{dt} = \frac{9.8\kappa^3}{\nu}\frac{U_0^2}{z^2(e^z - 1)} \quad \ldots\ldots (17)$$

At small values of t, Eq. 17 can be written as

$$\frac{dz}{dt} = \frac{9.8\kappa^3}{\nu} U_{1m}^2 \frac{\omega^2 t^2}{z^3} \quad \ldots\ldots (18)$$

which has the solution

$$z = \sqrt[4]{\frac{4}{3}\alpha(\omega t)^3} = t_1^* \quad \ldots\ldots (19)$$

$$\text{in which} \quad \alpha = \frac{9.8\kappa^3 U_{1m}^2}{\nu\omega} = 9.8\kappa^3 \mathsf{R} \quad \ldots\ldots (20)$$

Here, R is the "amplitude Reynold's number" (Ref. 9, p. 114) defined by

$$\mathsf{R} = \frac{U_{1m} a}{\nu} = \frac{U_{1m}^2}{\nu\omega} \quad \ldots\ldots (21)$$

As in the rough bed case, z increases infinitely fast with time at $t = 0$, so t must be replaced by t_1^*, Eq. 19, in the numerical solution of Eq. 17. The solution of z is quite similar to those presented in the rough bed case in Fig. 1, the parameter now being R instead of a/k. In Fig. 4, the variation in f_w, defined in Eq. 12, with the Reynold's number is shown and compared with Kamphuis' experimental results, which fit well with the formula $f_w = 0.065\mathsf{R}^{-0.2}$ [Jonsson (9), p. 128, suggested $f_w = 0.09\,\mathsf{R}^{-0.2}$].

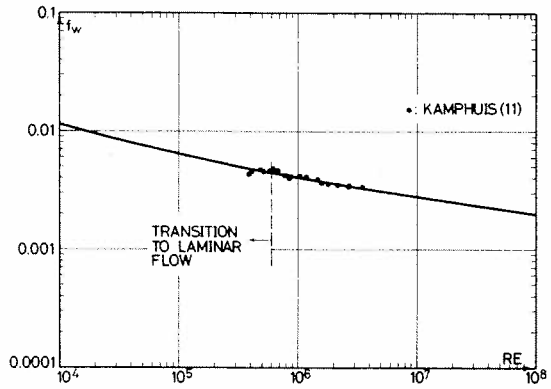

FIG. 4.—Variation in Friction Factor with Reynold's Number in Case of Smooth Bed

For values of R smaller than about $5 \times 10^{+5}$, we have transition between laminar and smooth turbulent transition (Ref. 9, p. 117).

In Table 2, the variation of phases ϕ and boundary layer thickness δ_w, defined as in the rough bed case, is given as a function of R.

Combined Wave Current Motion

Kinematic Description.—In the present section, the ideas developed for the pure wave boundary layer is extended to cover the general motion of combined wave-current motion in the case of a rough bed, which is the most common in nature. Now, the instantaneous velocity profile $\vec{U}$ consists of two parts: a steady component, $\vec{U}_1$, due to the mean current and an unsteady component, $\vec{U}_2$, due to the wave motion.

The unsteady component is described in the same way as in the previous section: outside a small boundary layer at the bottom, still called the wave boundary layer, the velocity from the unsteady flow is calculated by potential theory, so in case of a sinusoidal wave the velocity is just outside the boundary layer given by Eq. 2. Inside the boundary layer, the unsteady part of the velocity is assumed to be logarithmic and given by Eq. 3.

The steady component, $\vec{U}_1$, is described as follows: outside the wave

TABLE 2.—Variation in Boundary Layer Thickness and Phase in Case of Smooth Wall

R (1)	δ_1/a (2)	ϕ, in degrees (3)
10^4	0.0322	13
10^5	0.0232	10
10^6	0.0176	8
10^7	0.143	6.3
10^8	0.114	5.5

boundary layer the turbulence is due to the mean current only. Here, the usual logarithmic velocity distribution

$$\frac{U_1}{U_{fc}} = \frac{1}{\kappa} \ln \frac{y}{\left(\frac{k_w}{30}\right)} \quad \text{(22)}$$

is adopted. k_w stands for an apparent bed roughness which is different from the grain roughness as the wave boundary layer acts as a larger roughness element. U_{fc} in Eq. 22 stands for the current friction velocity to be determined later.

Inside the wave boundary layer, the mean current velocity profile is assumed to be given by

$$\frac{U_1}{U_{f0}} = \frac{1}{\kappa} \ln \frac{y}{\left(\frac{k}{30}\right)} \quad \text{(23)}$$

The boundary condition at the top of the wave boundary layer ($y = \delta + k/30$) is that the vectorial sum of the potential flow velocity (Eq. 2) and the mean current profile (Eq. 23) is equal to the instantaneous velocity at $y = \delta + k/30$ given by Eq. 3. If the angle between mean current direction and direction of wave propagation is called γ, this condition becomes

$$\left[\frac{U_f}{\kappa} \ln \left(\frac{\delta + \frac{k}{30}}{\frac{k}{30}}\right)\right]^2 = \left[\frac{U_{f0}}{\kappa} \ln \left(\frac{\delta + \frac{k}{30}}{\frac{k}{30}}\right) + U_0 \cos \gamma\right]^2$$

$$+ [U_0 \sin \gamma]^2 \quad \text{(24)}$$

cf. Fig. 5, where U_δ stands for the mean current velocity at the distance, δ, above the bed (given by Eq. 23).

If, as in Eq. 6, we introduce a quantity, z by

$$z = \frac{\kappa U_0}{U_f^*} \quad \text{(25)}$$

in which U_f^* in the present case is given by

$$\frac{1}{U_f^*} = \frac{U_{f0} \cos \gamma}{U_f^2 - U_{f0}^2} + \sqrt{\frac{U_{f0}^2 \cos^2 \gamma}{(U_f^2 - U_{f0}^2)^2} + \frac{1}{U_f^2 - U_{f0}^2}} \quad \text{(26)}$$

we obtain from Eq. 24 the same relationship as in Eq. 5:

$$\delta = \frac{k}{30}(e^z - 1) \quad \text{(27)}$$

Finally, the angle ϕ between the instantaneous flow direction in the boundary layer and the mean current direction (Fig. 5) is needed for use later on: from Fig. 5 it is seen that

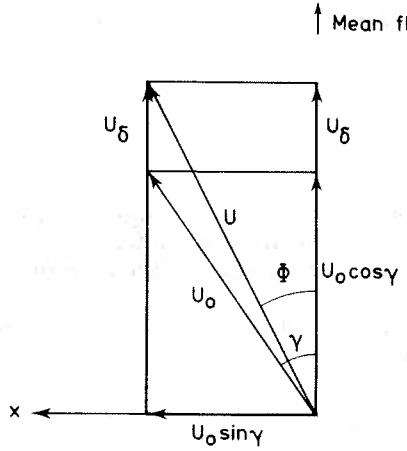

FIG. 5.—Definition Sketch of γ and Φ

$$\cos\Phi = \frac{U_0 \kappa \cos\gamma + U_{f0} \ln z}{U_f \ln z} \quad \ldots\ldots (28)$$

Finally, $$\sin\Phi = \frac{U_f^*}{U_f} \sin\gamma \quad \ldots\ldots (29)$$

is obtained from Eq. 28 by use of Eqs. 26 and 27.

Dynamic Description.—The momentum equation applied on the boundary layer in the direction perpendicular to the mean current direction (the x-direction, see Fig. 5) is given by

$$\int_{k/30}^{\delta+k/30} \rho \frac{d}{dt}(U \sin\Phi - U_0 \sin\gamma)dy = -\tau_b \sin\Phi \quad \ldots\ldots (30)$$

in which the first term on the left-hand side under the integral sign stands for the acceleration in the z-direction, the next term is the pressure gradient from the wave outside the wave boundary layer. The right-hand side of Eq. 30 represents the bed shear stress component in the x-direction.

The principle in the study of the wave boundary layer development is the same as in the previous study of the pure wave boundary layer: the development of the boundary layer for $0 \leqq \omega t \leqq \pi$ is first studied. At $t = 0$, the flow picture is identical with the resulting mean current velocity profile, U_0 being zero, and the effect of eddies formed by the previous movement being disregarded. At $\omega t = \pi$, we return to the original flow situation ($U_0 = 0$) and a new wave boundary layer, similar to the former one, will develop during the next half wave period.

The development is calculated from Eq. 30, in which Eq. 29 is inserted. After integration of Eq. 30, we get

$$-U_f U_f^* + \frac{k}{30}(e^z - 1)\frac{dU_0}{dt} = \frac{k}{30\kappa}[e^z(z-1)+1]\frac{dU_f^*}{dt} \quad \ldots\ldots (31)$$

U_f^* is defined in Eq. 25, from which we obtain (like Eq. 8)

$$\frac{dU_f^*}{dt} = \frac{U_f^*}{U_0}\frac{dU_0}{dt} - \frac{U_f^*}{z}\frac{dz}{dt} \quad \ldots\ldots (32)$$

Inserting Eq. 32 into Eq. 31, we get after some rearrangements

$$\frac{dz}{dt} = \frac{z(1+z-e^z)}{e^z(z-1)+1}\frac{1}{U_0}\frac{dU_0}{dt} + \frac{30\kappa}{k}\frac{\sqrt{\kappa^2 U_0^2 + z^2 U_{f0}^2 + 2z\kappa U_{f0} U_0 \cos\gamma}}{e^z(z-1)+1} \quad \ldots (33)$$

Like Eq. 9, Eq. 33 is singular at $t = 0$, which by Taylor expansion can be written as

$$\frac{dz}{d(\omega t)} = \beta_1 \left\{ \left[\frac{1}{z} + \frac{\kappa^2}{2}\left(\frac{U_{1m}}{U_{f0}}\right)^2 \frac{(\omega t)^2}{z^3} \right] + \kappa \frac{U_{1m}}{U_{f0}} \frac{\omega t}{z^2} \cos\gamma \right\} - \frac{z}{\omega t} \quad \ldots\ldots (34)$$

in which $$\beta_1 = \frac{60\kappa\, U_{f0}}{\omega k} \quad \ldots\ldots (35)$$

The solution to Eq. 34 at small values of ωt is

$$z = \sqrt{\frac{2}{3}\beta_1}\sqrt{\omega t} \quad \ldots\ldots (36)$$

Eq. 35 must be solved numerically for larger values of ωt.

The variation in z depends on the two parameters β_1 and U_{1m}/U_{f0}. However, β_1 can be written as (cf. Eq. 35)

$$\beta_1 = 60\kappa \frac{U_{1m}}{k}\frac{U_{f0}}{U_{1m}} = 60\kappa \frac{\frac{a}{k}}{\frac{U_{1m}}{U_{f0}}} \quad \ldots\ldots (37)$$

in which a = the free stream particle amplitude. Thus, alternatively z depends on the two quantities a/k and U_{1m}/U_{f0}.

In Fig. 6, an example of the variation in U_f and the boundary layer thickness δ is shown for specific values of a/k and U_{1m}/U_{f0} for the special case where the direction of wave propagation is the same as the mean current direction. (In Fig. 6 ϕ_+ is the phase between the maximum shear stress and maximum velocity; and ϕ_- is the phase between minimum shear stress and minimum velocity.)

Having obtained the variation in U_f with time, the momentum equation applied in the mean flow direction (Fig. 5) gives the mean bed shear $\bar{\tau}$ in this direction. The momentum equation in this direction is

$$\int_{k/30}^{\delta+k/30} \rho \frac{d}{dt}(U \cos\Phi - U_0 \cos\gamma)dy = -\tau_b \cos\Phi + \tau \quad \ldots\ldots (38)$$

in which τ stands for the current shear stress outside the wave boundary layer, which is directed in the x-direction. Integration of Eq. 38 with respect to time over one wave period yields

$$\bar{\tau} = \rho U_{fc}^2 = \int_0^T \tau_b \cos\Phi\, dt = \int_0^T \rho U_f^2 \cos\Phi\, dt \quad \ldots\ldots (39)$$

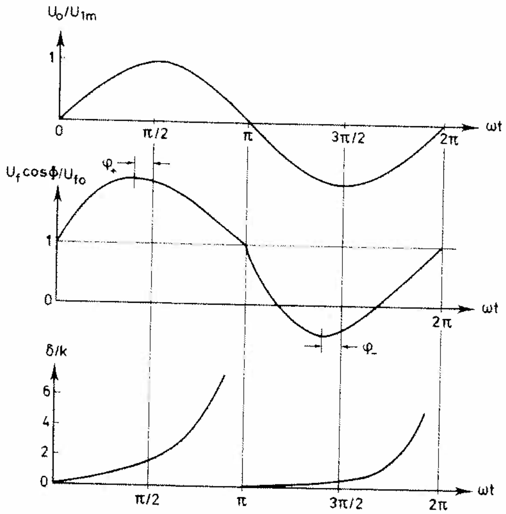

FIG. 6.—Variation in U_0, U_f, and δ During Wave Period for a/k = 10 and U_{1m}/U_{f0} = 10

because the left-hand side of Eq. 38 becomes zero when it is integrated over a wave period (no acceleration of the mean flow velocity).

The apparent roughness, k_w, is determined by matching the inner and the outer mean current profile in the mean thickness of the boundary layer, δ_m, which from Eqs. 22–23 gives

$$\frac{k_w}{k} = \left(\frac{30\delta_m}{k}\right)^{1-U_{f0}/U_{fc}} \quad \text{(40)}$$

in which δ_m is in the present taken as the mean value of $\delta(\omega t = \pi/2)$ and $\delta(\omega t = 3\pi/2)$ (Fig. 6).

Theoretical Results

In Fig. 7 the variations in k_w/k as the function of U_{1m}/U_{fc} are depicted for different values of a/k.

Fig. 7(*a*) shows the variation for $\gamma = 0°$, while Fig. 7(*b*) shows the similar variation for $\gamma = 90°$. It is interesting to note that the curves cross each other, which means that the apparent roughness at strong current (small values of U_{1m}/U_{fc}) is largest at small values of a/k (that means fast oscillations), while the reverse is the case at weak current. In Fig. 8, a comparison is made between the apparent bed roughness for two and three dimensional flow for the same value of a/k.

It turns out that the apparent roughness is always the largest for two dimensional flow.

In Fig. 9, the variation in δ_m/k with U_{1m}/U_{fc} is shown for both 2-*D* (γ = 0°) and 3-*D* (γ = 90°) flow: The variations turn out to be nearly identical, the three dimensional boundary layer being slightly larger than the two dimensional except in the two limits (weak and strong current).

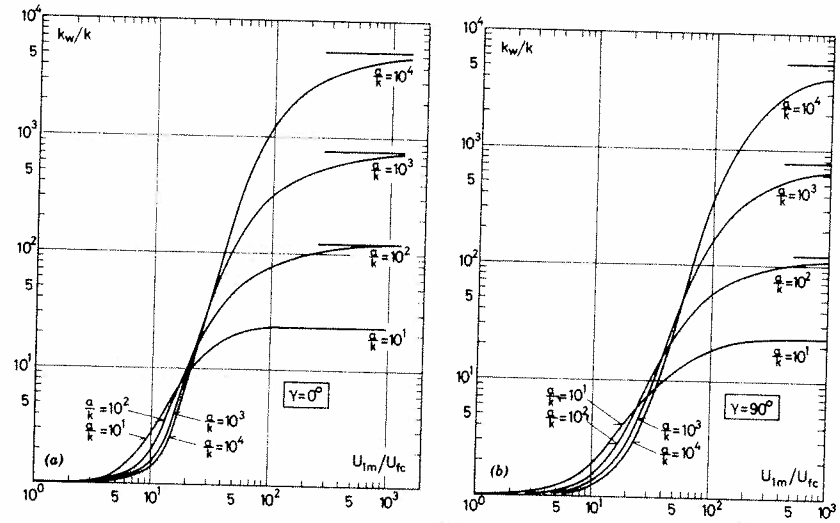

FIG. 7.—Variation in k_w/k with U_{1m}/U_{fc} for Different Values of a/k: (*a*) γ = 0°; (*b*) γ = 90°

Finally, Fig. 10 shows the variation in U_{fc}/U_{f0} with U_{1m}/U_{fc} for $\gamma = 0°$ and 90°. From these diagrams, Figs. 7, 9, and 10, it is easy to describe the flow as explained in the following.

Application of Diagrams and Comparison with Experiments

If the boundary layer thickness δ_m is small compared with the water depth, Eq. 2 yields

$$\frac{V}{U_{fc}} = \frac{1}{\kappa}\left[\ln\left(\frac{D}{\frac{k_w}{30}}\right) - 1\right] \quad \text{(41)}$$

in which V = the mean current velocity.

The diagrams depicted in Figs. 7, 9, and 10 are now applied in the following way:

Let us assume that V, D, U_{1m}, a, and k are known quantities. By choosing an initial value of U_{fc}, k_w can be found from Fig. 7. If the selected value of U_{fc} is not equal to that obtained from Eq. 41, a new value of U_{fc} must be chosen until agreement occurs.

If the inner solution is also of interest, U_{f0} is now easily found from Fig. 10. Only very few experiments are available to verify the theory, and all are carried out in the special case where $\gamma = 0°$. Brevik (3) and Kemp and Simons (12) have measured the velocity profile in the case of a hydraulic smooth bed, while Bakker and Doorn (2) have measured the velocity profile in the case of a hydraulic rough bed.

In Fig. 11, the present theoretical findings are compared with Bakker and Doorn's (2) measurements. The dotted lines indicate the inner and outer solutions. However, because the solution of the wave boundary

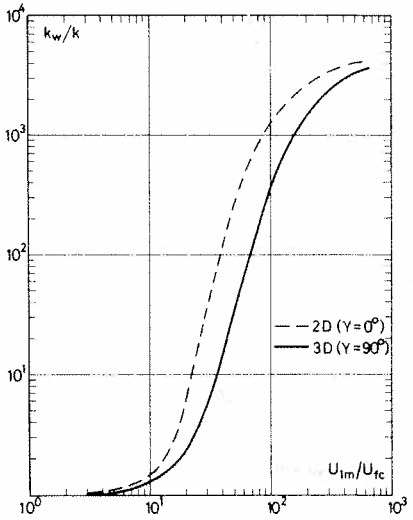

FIG. 8.—Variation in k_w/k with U_{1m}/U_{fc} for Two-Dimensional (Broken Line) and Three-Dimensional (Full-Drawn Line) Flow ($a/k = 10^4$)

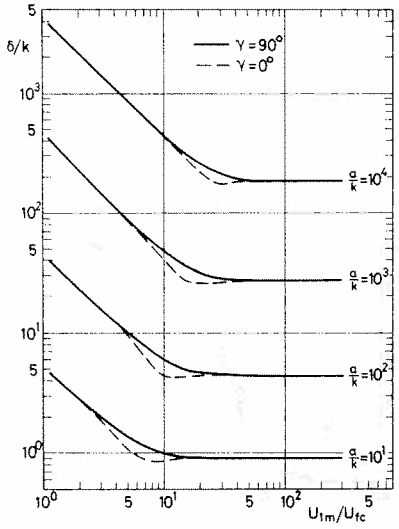

FIG. 9.—Variation in Wave Boundary Layer Thickness, δ/k, with U_{1m}/U_{fc}

layer is not totally symmetrical around the mean values, the correct mean profile is in fact not a logarithmic function, but instead the fully drawn line which is obtained by taking the average value of U over a wave period.

Variation in Friction Factor

From the graphs depicted in Figs. 7, 9, and 10, it is, furthermore, possible to determine the friction factor for the flow. The friction factor for the mean current motion is defined by

$$f_c = 2\left(\frac{U_{fc}}{V}\right)^2 \quad \ldots\ldots (42)$$

in which V/U_{fc} is found by Eq. 41. Thus, besides the data already given in Figs. 7, 9, and 10, it is necessary to know the dimensionless water depth, D/k. The variation in f_c is shown in Fig. 12 for $\gamma = 0°$ and $\gamma = 90°$ for a specific value of D/k and a/k: for strong current, f_c approaches f_{c0}, which is the friction factor in pure current, obtained from Colebrook-White's formula. For weak current, f_c increases to a higher value, which in the limit is given by

$$\sqrt{\frac{2}{f_c}} \to \frac{1}{\kappa}\ln\left(\frac{D}{\delta_w} - 1\right) \quad \ldots\ldots (43)$$

in which δ_w = the pure wave boundary layer thickness. From Fig. 12 it

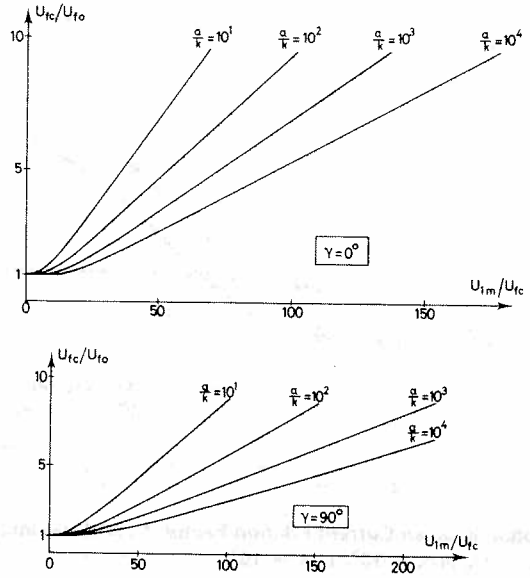

FIG. 10.—Variation in U_{fc}/U_{f0} with U_{1m}/U_{fc}

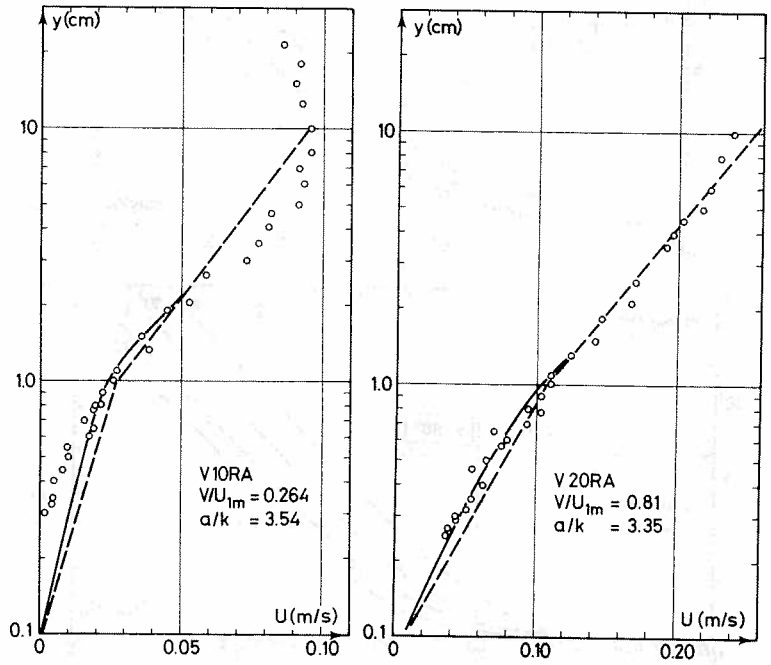

FIG. 11.—Comparison between Theory and Experiments by Bakker and Doorn (2); Numbering of Experiments Are from Ref. 2

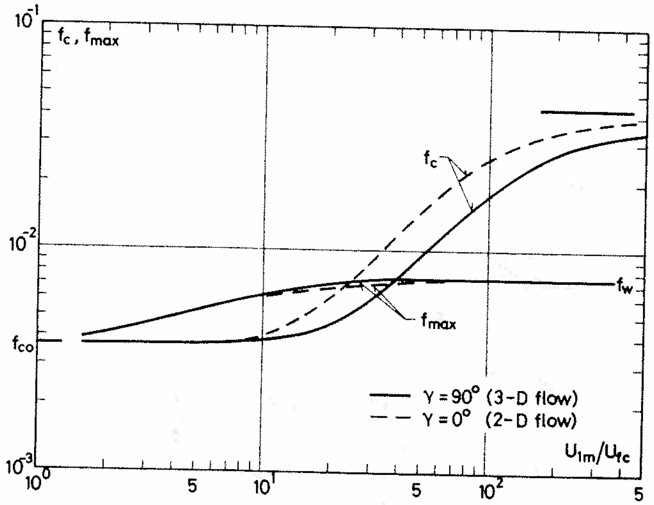

FIG. 12.—Variation in Mean Current Friction Factor, f_c, and Maximum Friction Factor, f_{max}, with U_{1m}/U_{fc} ($a/k = 10^3$; $D/k = 10^3$)

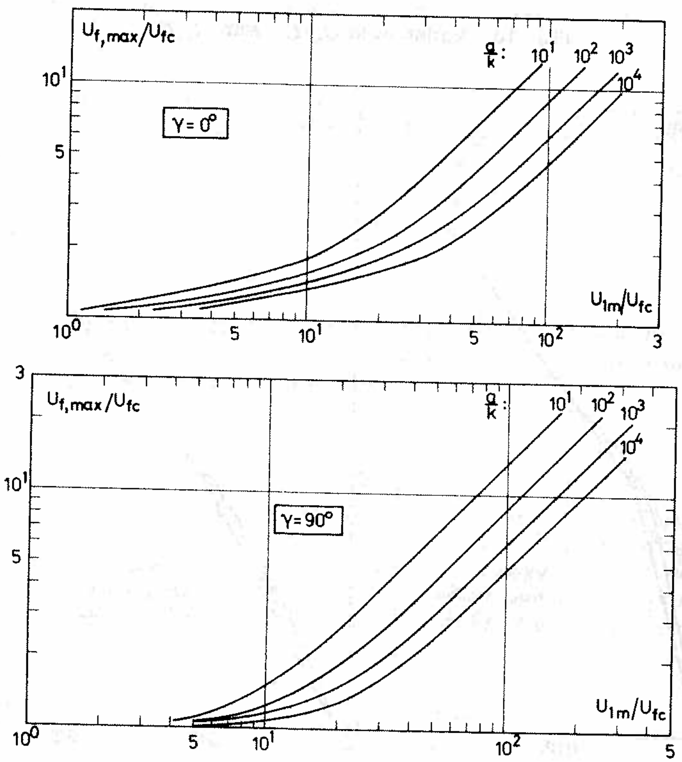

FIG. 13.—Variation in Maximum Shear Velocity with U_{1m}/U_{fc} for Different Values of a/k

is seen that the friction factor is largest for 2-*D* flow.

Besides the friction factor for the mean current flow, the maximum bed shear stress during a wave period is also of interest (for sediment transport). In Fig. 13, the variation in $U_{f,max}/U_{fc}$, in which $U_{f,max}$ = the maximum friction velocity during a wave cycle, is depicted as a function of U_{1m}/U_{fc} for different values of a/k. From this diagram, together with Fig. 10, it is easy to find the maximum bed shear stress.

By defining a friction factor by

$$f_{max} = 2\left(\frac{U_{f,max}}{U_{\delta,max}}\right)^2 \quad (44)$$

in which $U_{\delta,max}$ = the maximum flow velocity at the top of the boundary layer (the vectorial sum of wave velocity and mean current velocity); f_{max} can be evaluated from Fig. 13. An example of the variation in f_{max} is also shown in Fig. 12. At weak current, f_{max} approaches the wave friction factor f_w depicted in Fig. 2.

Conclusion

A model for the wave boundary layer in combined wave current has been developed which takes its starting point on a reasonable guess of the velocity profile inside and outside the wave boundary layer. By application of the momentum equation in the direction perpendicular to the mean current direction, the calculations are reduced to the solution of a first order ordinary differential equation. In the case of no mean current, the theoretical findings agree well with the measured friction factor in the rough bed case as well as in the smooth bed case. In the case of a nonvanishing mean current, the calculations are carried out only for a rough bed, where the calculated mean current profile agrees reasonably well with the measurements by Bakker and Doorn.

Appendix.—References

1. Bakker, W. T., "Sand Concentration in an Oscillatory Flow," Coastal Engineering Conference, 1974, pp. 1129–1148.
2. Bakker, W. T., and Doorn, T., "Near-Bottom Velocities in Wave with a Current," Coastal Engineering Conference, 1978, pp. 1394–1413.
3. Brevik, I., "Flume Experiments on Waves and Currents Above a Smooth Bed," *Report 9*, Trondheim University, Division of Port and Ocean Engineering, 1979.
4. Brevik, I., "Oscillatory Rough Turbulent Boundary Layers," *Journal of the Waterway, Port and Ocean Division*, ASCE, Vol. 107, No. WW3, 1981, pp. 175 and 188.
5. Fredsøe, J., "Mean Current Velocity Distribution in Combined Waves and Current," *Progress Report No. 53*, ISVA, Technical University of Denmark, 1981, pp. 21–26.
6. Grant, W. D., and Madsen, O. S., "Combined Wave and Current Interaction with a Rough Bottom," *Journal of Geophysical Research*, Vol. 84, 1979, pp. 1797–1808.
7. Jonsson, I. G., "Measurements in the Turbulent Wave Boundary Layer," IAHR, 10th Congr. 1, London, 1963, pp. 85–92.
8. Jonsson, I. G., and Carlsen, N. A., "Experimental and Theoretical Investigations in an Oscillatory Turbulent Boundary Layer," *Journal of Hydraulic Research*, Vol. 14, No. 1, 1976, pp. 45–60.

9. Jonsson, I. G., "A New Approach to Oscillatory Rough Turbulent Boundary Layers," *Ocean Engineering*, Vol. 7, 1980, pp. 109–152, tables in No. 4, pp. 567–570.
10. Kajiura, K., "A Model of the Bottom Boundary Layer in Water Waves," *Bulletin of the Earthquake Research Institute*, Vol. 46, 1968, pp. 75–123.
11. Kamphuis, J. W., "Friction Factor under Oscillatory Waves," *Journal of the Waterway, Port and Ocean Division*, ASCE, Vol. 101, No. WW2, 1975, pp. 135–144.
12. Kemp, P. H., and Simons, R. R. "The Interaction Between Waves and a Turbulent Current: Waves Propagating with the Current," *Journal of Fluid Mechanics*, Vol. 116, 1982, pp. 227–250.
13. Lundgren, H., "Turbulent Currents in the Presence of Waves," *Coastal Engineering Conference*, 1972, pp. 623–634.

Two-Dimensional Flood Routing on Steep Slopes[a]

By Robert A. Laura,[1] A. M. ASCE and John D. Wang,[2] M. ASCE

Abstract: Program ROUTWEIR represents a two-dimensional flood routing model designed to analyze two-dimensional flow caused by rainfall and runoff flooding events. Input to the program consists of known geometry, topography, initial conditions, and boundary conditions. The geometry and bathymetry of the flood plain are represented by a grid of interconnecting triangular elements. Initial water levels are prescribed to correspond to the normal water elevations in the river channel. Boundary conditions are prescribed by a discharge hydrograph at the upstream boundary of the river basin, and by the water surface elevations at the ocean boundary. The interior water elevations and discharges are computed, allowing flooding and drying to take place in the triangular elements of the grid, based on a conservation of water volume equation and a surface slope dependent dynamic equation. Output consists of time histories of water surface elevations and peak elevations in both tabular and graphical form. ROUTWEIR has been successfully calibrated against recorded flood levels in the Rio Culebrinas Basin in Puerto Rico and has been used in that basin in a federal flood insurance study. A versatile computer program, ROUTWEIR can be applied to many flood routing problems. It is particularly suited for wide river basins with large bottom slopes and for normally dry areas subject to extensive flooding.

Introduction

The two-dimensional flood routing model, Program ROUTWEIR, was designed to analyze flow caused by rainfall and runoff flooding events in complex river basins where one-dimensional programs, such as HEC-2 (8), do not apply. This computer model was developed under a Federal Emergency Management Agency (FEMA) contract for use in a flood insurance study (5), which investigated the existence and severity of flood hazards in the Culebrinas River Basin in Puerto Rico.

The impetus to develop this particular model arose from the rather special conditions encountered in Puerto Rican river basins. These basins are characterized by steep longitudinal gradients in topography and by severe storms that cause extensive flooding of the river banks and adjacent land. As a flood wave propagates through this system, numerous transitions from supercritical to subcritical flow and vice versa may take place at different times and locations. Also, the transverse flow over river banks and onto dry land greatly affects maximum flood elevations.

Existing models such as HEC-2 (8) and WSP-2 (6) have brought the

[a]Presented at the Sept. 2–5, 1982, ASCE Joint Florida/South Florida Annual Meeting, "Engineering for the 21st Century," held in Orlando, Fla.
[1]Sr. Engr., Post, Buckley, Schuh & Jernigan, Inc., Miami, Fla.
[2]Assoc. Prof., Div. of Ocean Engrg., Rosenstiel School of Marine and Atmospheric Sci., Univ. of Miami, Miami, Fla.
Note.—Discussion open until January 1, 1985. To extend the closing date one month, a written request must be filed with the ASCE Manager of Technical and Professional Publications. The manuscript for this paper was submitted for review and possible publication on April 29, 1983. This paper is part of the ***Journal of Hydraulic Engineering***, Vol. 110, No. 8, August, 1984. ©ASCE, ISSN 0733-9429/84/0008-1121/$01.00. Paper No. 19058.